Large Eddy Simulation of Cylindrical Jet Breakup and Correlation of Simulation Results With Experimental Data

Shashank S. Moghe[1]
Mem. ASME
MAHLE Engine Components USA Inc.,
23030 MAHLE Drive,
Farmington Hills, MI 48335
e-mail: shashank.moghe@us.mahle.com

Scott M. Janowiak
MAHLE Engine Components USA Inc.,
23030 MAHLE Drive,
Farmington Hills, MI 48335
e-mail: scott.janowiak@us.mahle.com

Modern engines with increasing power densities have put additional demands on pistons to perform in incrementally challenging thermal environments. Piston cooling is therefore of paramount importance for engine component manufacturers. The objective of this computational fluid dynamics (CFD) study is to identify the effect of a given piston cooling nozzle (PCN) geometry on the cooling oil jet spreading phenomenon. The scope of this study is to develop a numerical setup using the open-source CFD toolkit OpenFoam® for measuring the magnitude of oil jet spreading and comparing it to experimental results. Large eddy simulation (LES) turbulence modeling is used to capture the flow physics that affects the inherently unsteady jet breakup phenomenon. The oil jet spreading width is the primary metric used for comparing the numerical and experimental results. The results of simulation are validated for the correct applicability of LES by evaluating the fraction of resolved turbulent kinetic energy (TKE) at various probe locations and also by performing turbulent kinetic energy spectral analysis. CFD results appear promising since they correspond to the experimental data within a tolerance (of ±10%) deemed satisfactory for the purpose of this study. Further generalization of the setup is underway toward developing a tool that predicts the aforementioned metric—thereby evaluating the effect of PCN geometry on oil jet spreading and hence on the oil catching efficiency (CE) of the piston cooling gallery. This tool would act as an intermediate step in boundary condition formulation for the simulation determining the filling ratio (FR) and subsequently the heat transfer coefficients (HTCs) in the piston cooling gallery.
[DOI: 10.1115/1.4036528]

Keywords: CFD, OpenFoam®, large eddy simulation

Introduction

Modern day engines and those under development for the future are growing incrementally aggressive in terms of increasing the power densities and progressive downsizing. Increasing power densities imply a greater thermal load on the power cell components, with one of the most prominently affected components being the piston [1]. Downsizing also has a severe impact on the design of the piston since there is a greater spatial restriction on the structural and thermal reinforcements that can be accommodated in the design. From the standpoint of an engine component manufacturer, cooling performance of the piston under such enhanced thermal loads therefore becomes a primary focus for new product development.

The design of the piston cooling gallery is dependent on several factors—the oil jet characteristics, the cooling gallery inlet and outlet geometry, and the inside geometry of the cooling gallery itself. The contribution of these variables toward gallery design is grouped broadly into two metrics: CE and FR.

The catching efficiency is defined as the fraction of the oil exiting the PCN that enters the piston cooling gallery. This metric captures the combined effect of the cooling gallery inlet geometry design and oil jet spreading

$$\mathrm{CE} = \left(\frac{\text{oil inflow at the gallery inlet} - \text{oil backflow at the gallery inlet}}{\text{oil outflow at the PCN}} \right) \tag{1}$$

The filling ratio is defined as the fraction of the piston cooling gallery volume that is filled with oil. This metric captures the combined effect of the cooling gallery inlet and outlet geometry design as well as the design of the inside-gallery geometry and the piston motion dynamics

[1]Corresponding author.

Contributed by the IC Engine Division of ASME for publication in the Journal of Engineering for Gas Turbines and Power. Manuscript received February 14, 2017; final manuscript received March 24, 2017; published online May 16, 2017. Editor: David Wisler.

$$\mathrm{FR} = \left(\frac{\text{volume of oil in the cooling gallery}}{\text{volume of the cooling gallery}}\right) \tag{2}$$

These metrics aid in deciding upon the potency of a particular piston cooling gallery design. Combined with the empirical relations developed for the prediction of thermal performance of a piston as a function of the filling ratio and cooling gallery oil throughput, these metrics assume a decisive role in determining the suitability of a particular piston design against the engine application specific thermal load. It is necessary to identify the values of these metrics whenever a new piston design is conceptualized. Development of a computational tool to serve this purpose therefore provides a twofold advantage—accelerate the process of new product development and be comparatively less expensive than experimental validation.

To begin with a piston cooling gallery design feasibility study, the natural starting point is the determination of cooling oil jet spreading characteristics. As a power cell unit (PCU) component manufacturer, only the dimensions of the PCN along with its relative location to the piston are provided by the customers. To design an optimal piston cooling gallery, knowledge of the oil jet spreading width at different heights of the stroke becomes indispensable since it dictates the catching efficiency of the piston cooling gallery. The variation of the catching efficiency with piston stroke acts as input data for the filling ratio CFD simulation. It is therefore necessary to develop a simulation tool that accurately predicts the oil jet spreading characteristics (spreading width). Such a tool has been developed based on the open-source CFD code OpenFoam® (version 2.4.x) and the primary objective of this work is to gauge the efficiency of this tool by comparison of the simulation predicted oil jet spreading width against experimental data.

The cylindrical jet is a case of an inherently unsteady, free shear flow where the turbulence is induced primarily because of the mean velocity differences [2]. Instability theories explain the mechanism of evolution of instabilities on the free surface and their interaction with the flow field leading to jet breakup. Kelvin–Helmholtz (KH) instability occurs when fluids of different densities have a relative motion at the interface. Instabilities start developing on the free surface due to the combined effect of the relative velocity at the interface and the surface tension between the fluids. According to the KH instability theory, a shear layer is formed between the jet and the surrounding fluid immediately downstream of the PCN exit [3]. Instabilities in the shear layer corresponding to certain frequencies (depending on the Reynolds number of the flow and interfacial surface tension) are amplified exponentially. These amplified instabilities interact with the surrounding fluid resulting in the formation of vortices in a phenomenon called "vortex roll-up" [4,5], documented in literature by experimental observations [6,7]. Through nonlinear interactions, these vortices pair and result in the formation of large-scale structures further downstream in the flow field—entraining the surrounding fluid into the jet bulk—ultimately leading to the breakup of the jet.

The use of LES is justified in the modeling of free shear flows like the cylindrical oil jet breakup, where the flow transport phenomena of interest are governed by the large scales of turbulence [8]. LES is a turbulence modeling approach where the large scales of turbulence—representing a major fraction of the TKE—are resolved, while the significantly smaller dissipative scales are modeled using a suitable subgrid scale (SGS) model. The one-equation-eddy SGS model is used in the present study. Correct applicability of the LES approach is verified using the LES quality metric [8] (that represents the fraction of the TKE resolved by the simulation) in accordance with Pope's guideline of a suggested minimum 80% resolution of the TKE [2]. The rate of energy cascade—transfer of TKE from the larger energy producing scales to the smaller scales—is verified by performing energy spectral analysis on the test case data. The Governing Equations: LES and SGS Modeling sections provide a brief detail on the LES approach and SGS modeling.

Governing Equations: LES

The mathematical form of the governing equations of fluid dynamics is provided by the collective set of the continuity equation and the momentum equations (also referred to as the Navier–Stokes equations). The continuity and Navier–Stokes equations take the following form (in the Einstein notation) for incompressible flow in the absence of any external source/sink (except gravity):

Continuity equation

$$\frac{\partial u_i}{\partial x_i} = 0 \tag{3}$$

Momentum equation

$$\frac{\partial u_i}{\partial t} + \frac{\partial u_i u_j}{\partial x_j} = -\frac{1}{\rho}\frac{\partial p}{\partial x_i} + \nu\left(\frac{\partial^2 u_i}{\partial x_j \partial x_j}\right) + g_i \tag{4}$$

where u_i and u_j represent the components of velocity over the three spatial dimensions, p represents the pressure, g_i represents the component of acceleration due to gravity, ν represents the kinematic viscosity, and ρ represents the density of the fluid. The momentum equation representation in Eq. (4) assumes a spatially invariant kinematic viscosity and density of the fluid.

LES adopts the methodology of resolving the largest scales of turbulence—which are anisotropic in nature and contain a majority fraction of the TKE—and modeling the smaller scales—which are isotropic and dissipative in nature. Consider a scalar function $\varphi(x)$ represented according to the LES methodology as comprised of the resolved and modeled parts

$$\varphi(x) = \overline{\varphi}(x) + \varphi'(x) \tag{5}$$

where $\overline{\varphi}(x)$ and $\varphi'(x)$ represent the spatially resolved (filtered) contribution corresponding to the energy containing large scales of turbulence and the modeled contribution corresponding to the significantly smaller dissipative scales of turbulence, to $\varphi(x)$, respectively. The dissipative scales of turbulence are statistically similar irrespective of the flow geometry under consideration. Therefore, these scales are modeled while the flow-dependent larger scales of turbulence are resolved.

Spatial filtering of flow variables in LES is accomplished with the help of a filter function $G(x_i, x_i')$ which, if uniform, is independent of the spatial position x_i The uniform filter function must satisfy the normalization condition

$$\int_{\mathrm{FV}} G(x_i')\mathrm{d}x_i' = 1 \tag{6}$$

The OpenFoam® default top-hat spatial filter function is used in this study, defined as

$$\begin{aligned} G(x_i') &= \frac{1}{\Delta} \ \text{ if } |x_i'| \le \frac{\Delta}{2} \\ G(x_i') &= 0 \ \text{ otherwise} \end{aligned} \tag{7}$$

In Eq. (7), Δ is the spatial filter cutoff width. An LES can employ explicit filtering where Δ is explicitly defined or implicit filtering where Δ is associated with the mesh dimensions. In the present CFD study, implicit spatial filtering has been adopted with the spatial filter cutoff width defined as

$$\Delta = \text{cell volume}^{\frac{1}{3}} \tag{8}$$

The spatial filtering operation performed on the scalar function $\varphi(x)$—yielding $\overline{\varphi}(x)$—is defined as

$$\overline{\varphi}(x) = \int_{\text{FV}} G(x_i') \cdot \varphi(x - x_i') dx_i' \tag{9}$$

Applying the filtering operation on the continuity and momentum equations (neglecting any external source/sink terms) for incompressible flow yields the following form derived for LES:

$$\frac{\partial \overline{u}_i}{\partial x_i} = 0 \tag{10}$$

$$\frac{\partial \overline{u}_i}{\partial t} + \frac{\partial \overline{u}_i \overline{u}_j}{\partial x_j} = -\frac{1}{\rho}\frac{\partial \overline{p}}{\partial x_i} + \nu\left(\frac{\partial^2 \overline{u}_i}{\partial x_j \partial x_j}\right) - \frac{\partial \tau_{ij}}{\partial x_j} \tag{11}$$

τ_{ij} is the SGS stress tensor that needs to be modeled and represents the contribution of the smaller scales of turbulence that are not resolved by the mesh. It is defined as

$$\tau_{ij} = \overline{u_i u_j} - \overline{u}_i \overline{u}_j \tag{12}$$

SGS Modeling

The last term in Eq. (11) containing the SGS stress tensor represents the contribution of the unresolved scales in the flow domain and demands a correlation to the resolved flow for closure of the system of equations. The eddy-viscosity based approach is used to correlate the deviatoric part of the SGS stress tensor to the resolved scales (represented by the filtered strain-rate tensor $\overline{S}_{ij}$)

$$\tau_{ij} - \frac{1}{3}\tau_{kk}\delta_{ij} = -2\nu_{\text{sgs}}\overline{S}_{ij} \tag{13}$$

$$\overline{S}_{ij} = \frac{1}{2}\left(\frac{\partial \overline{u}_i}{\partial x_j} + \frac{\partial \overline{u}_j}{\partial x_i}\right) \tag{14}$$

The eddy-viscosity approach based SGS models assume instantaneous and complete dissipation of all the TKE transferred from the resolved scales, implying equilibrium at the SGS. Zero-equation models (like the Smagorinsky model [9]) yield less accurate results in cases where this assumption becomes less applicable—such as free shear flows. This problem is resolved by the use of one-equation models which additionally solve a transport equation for one of the SGS turbulence variables [10].

In the one-equation-eddy SGS model used in this study, the SGS turbulent (eddy) viscosity ν_{sgs} is given as

$$\nu_{\text{sgs}} = c_k \Delta k_{\text{sgs}}^{\frac{1}{2}} \tag{15}$$

The model employs a transport equation for the SGS TKE (k_{sgs})—forcing accountability on the flow of TKE between the resolved and unresolved scales. The transport equation for k_{sgs} is given (as per OpenFoam® source code) as

$$\frac{\partial}{\partial t}k_{\text{sgs}} + \frac{\partial}{\partial x_i}u_i k_{\text{sgs}} = G - \frac{c_e k_{\text{sgs}}^{\frac{3}{2}}}{\Delta} + \frac{\partial}{\partial x_i}\left(\nu_{\text{effective}}\frac{\partial}{\partial x_i}k_{\text{sgs}}\right) \tag{16}$$

$$\nu_{\text{effective}} = \nu_{\text{sgs}} + \nu_{\text{molecular}} \tag{17}$$

where G is the rate of TKE transfer from the resolved scales to the SGS, given by

$$G = 2\nu_{\text{sgs}}|\overline{S}|^2 \tag{18}$$

$$\overline{S} = \left(2\overline{S}_{ij}\overline{S}_{ij}\right)^{\frac{1}{2}} \tag{19}$$

The second and third terms on the right-hand side of Eq. (16) represent the SGS TKE dissipation and diffusion, respectively. In the present study, OpenFoam® default values are used for the dimensionless constants c_k (0.094) and c_e (1.048).

Numerical Methods

To model the two-phase cylindrical oil jet breakup phenomenon in OpenFoam®-2.4.x, the isothermal interFoam solver based on the volume of fluid (VOF) method is used. The fluids (oil and air) are treated as immiscible and incompressible. The interface between oil and air is modeled using a phase-fraction weighted interface capturing approach. For pressure–velocity coupling the solver uses the PIMPLE algorithm—a blend of the pressure implicit with splitting of operators (PISO) [11] algorithm that allows for a non-iterative procedure to solve for the velocity field in unsteady problems and the semi-implicit method for pressure-linked equations (SIMPLE) [12] algorithm that is iterative and suitable for steady-state problems. The PIMPLE algorithm allows for an iterative approach (as employed in the SIMPLE algorithm) enveloping the predictor–corrector step (as employed in the PISO algorithm) for the calculation of unsteady pressure and velocity fields. The iterative approach allows for the use of a larger time-step (as compared to the PISO algorithm) while maintaining stability, as convergence is achieved at each time-step. OpenFoam® allows for the specification of the number of iterations and corrector steps to be employed at each time-step (specifying a single iteration reduces the PIMPLE algorithm to PISO). In the present study, the solver is run in the PISO mode with a Courant Number limit of 0.4 and 2 corrector steps.

First-order numerical schemes for discretizing the derivatives are more stable but less accurate and highly dissipative, thereby introducing numerical viscosity into the solution. The issue of numerical viscosity is severe because it adds to the effective viscosity, thereby additionally diffusing field gradients and making the solution less physically accurate. Reduction of numerical diffusion is imperative in the context of the present study since the aim is to simulate an unsteady free shear flow and large gradients (both temporal and spatial) are to be expected in the flow field. The present study adopts the usage of second-order numerical schemes in discretizing the spatial derivative terms. For temporal discretization in OpenFoam®, the second-order Crank–Nicolson scheme provides for a blending factor that allows using a blend of itself and the first-order Euler scheme. For the present study, a blending factor of 0.75 has been deemed optimal in providing a balance of accuracy and stability (blending factor of 1 corresponds to the pure second-order Crank–Nicolson approach and that of 0 corresponds to the pure first-order Euler approach).

Test Bench Setup

The test bench used for in-house experimentation is designed specifically to measure the spreading width of the oil jet at a specific height downstream of the PCN exit. The bench captures high-resolution images at a high frame-rate and the spreading width is ascertained by visual inspection of the images. Since automated image processing is not adopted, the visual method introduces an unquantified observational error in the measurement of the oil jet spreading width metric. Therefore, the goal of the present CFD study is to achieve a $\pm 10\%$ agreement with the experimentally observed values.

Three bench tests at different PCN inlet pressures (1 bar, 3 bar, and 5 bar) were performed for a single PCN geometry, henceforth

Fig. 1 Test bench for experimental determination of oil jet spreading

collectively referred to as configuration A. Oil jet spreading width measurements were obtained 283 mm downstream of the PCN exit—a distance corresponding to the top dead center (TDC) position of the piston for a particular engine application. The test bench is an open hydraulic circuit with a volume flow controlled pump and an oil tank. An oil flow meter and an oil pressure sensor are installed as part of the feedback mechanism. The bench tests are performed under steady-state conditions. The test bench is designed so as to allow for the oil to fall under the effect of gravity. Such a configuration facilitates better visual inspection of the oil jet spreading phenomenon. Figure 1 shows the test bench used for experimentation.

Simulation Case Setup

The CFD simulation case geometry is modeled after the experimental test bench setup. The three-dimensional case consists of a straight-run cylindrical PCN of diameter (d) 3.5 mm opening into a larger cylindrical plenum of diameter 60 mm and length 300 mm. A cylindrical domain approximately 17 times the diameter of the PCN is assumed to replicate the free atmospheric discharge condition for the oil jet in the bench tests. The schematic in Fig. 2 provides a two-dimensional perspective of the computational mesh.

Considering the large three-dimensional geometry and the mesh resolution requirements of LES, a refinement strategy is adopted to increase the mesh resolution in the region where the interaction of the oil jet with the surrounding air is expected. The snappyHexMesh utility (part of the OpenFoam® package) allows for the creation of a mesh from stereolithography (STL) files and provides for zonal mesh refinement options. Here, the central part of the cylinder is chosen to be divided into three concentric cylindrical subdomains of equal lengths and incremental radial dimensions to accommodate for the spreading oil–air interface as the oil jet travels downstream. The radii of these cylindrical subdomains are selected to entirely contain the oil jet within the bounds of these refinement zones. The mesh resolution is kept consistent in the refinement zones. The schematic in Fig. 3 provides a two-dimensional perspective of the zonal mesh refinement strategy.

The inlet pressures for configuration A bench tests were translated into the corresponding oil mass flow rates at the PCN inlet. Corresponding PCN inlet velocities were calculated for each case assuming incompressible flow (constant oil density). CFD simulation case details and fluid properties are documented in Tables 1 and 2, respectively.

A fine near-wall mesh resolution is required for LES to account for the effect of high-frequency eddies in the boundary layer. Since the aim of the present study is concentrated on identifying the effects of oil–air interaction much downstream of the PCN exit, wall interactions are neglected by the use of a coarser (than necessary) mesh near the PCN wall. In the context of the present study, it is assumed that the gain in computational speed due to a comparatively coarser mesh outweighs the loss of accuracy introduced due to the lack of a fine near-wall mesh resolution. Another assumption made here is that the primary contributors to the phenomenon of oil jet breakup are the natural surface instabilities and their aerodynamic interaction with the surrounding air.

A *no-slip* velocity boundary condition is imposed on the PCN wall. The PCN inlet is specified as a *turbulent-inlet* velocity boundary condition—allowing random temporal fluctuations about the mean (with user-defined amplitude)—attempting to

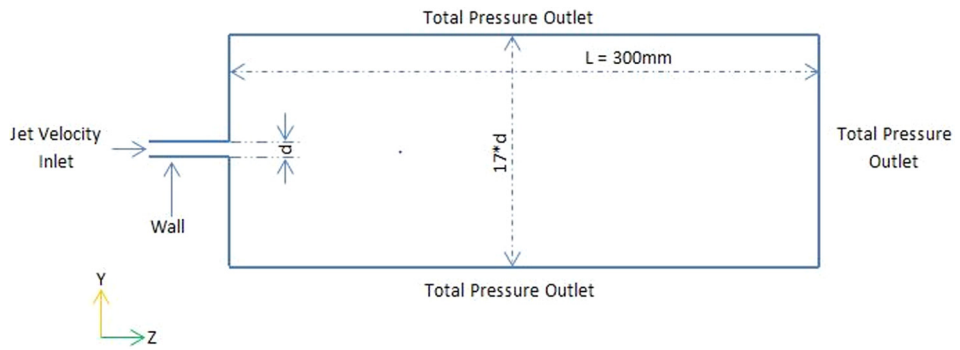

Fig. 2 Two-dimensional schematic for CFD simulation case setup

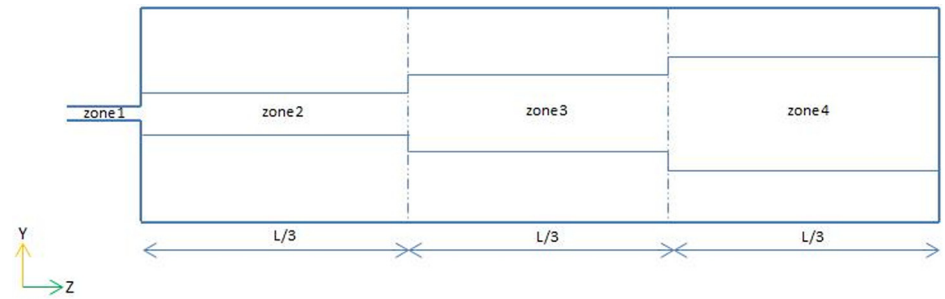

Fig. 3 Two-dimensional schematic for mesh refinement

Table 1 CFD simulation case details corresponding to configuration A bench tests

Case	PCN inlet pressure (bar gauge)	Flow rate (LPM)	Velocity (m/s)	Reynolds number (Re_{inlet})
A	1	6.30	10.84	2700
B	3	11.10	19.24	4800
C	5	14.40	24.96	6200

Table 2 Fluid properties

Property	Value
Oil density (ρ_{oil})	825 kg/m^3
Oil kinematic viscosity (ν_{oil})	1.4×10^{-5} m^2/s
Air density (ρ_{air})	1.184 kg/m^3
Air kinematic viscosity (ν_{air})	1.566×10^{-5} m^2/s
Oil–air surface tension (σ)	0.03 N/m

Table 3 Spreading width variation with U_z fluctuation magnitude

U_z fluctuation magnitude (%)	CFD spreading width at TDC (mm)
±1	29
±3	30
±5	30

Table 4 CFD simulation case boundary conditions

Patch	Velocity BC	Pressure BC
PCN inlet	Turbulent inlet	Zero gradient
PCN wall	No-slip	Zero gradient
Cylindrical plenum side, bottom, and outlet	Zero gradient	Total pressure

Table 5 Operational details of CFD test cases

Case	Mesh size	Number of cores	Run time (h)
1 bar	4.5×10^6 cells	48	55
3 bar		48	83
5 bar		72	87

replicate the oil mass flow rate fluctuations in the actual test bench. The velocity perturbations at the inlet are shown to have an effect on the formation of the large-scale turbulent structures in the flow field [3]. The present study does not impose nonstreamwise velocity fluctuations at the inlet. A random temporal fluctuation of ±5% amplitude in the streamwise component of velocity (U_z) was assumed for the purpose of this study to account for the velocity variations induced in the test bench PCN (the test bench PCN has a bend) due to the operational limitations of maintaining a constant pressure in the oil tank. A three-dimensional sensitivity study (considering only the 5 bar test case) was undertaken to identify the effect of the amplitude of the random temporal fluctuation in U_z on the oil jet spreading width. The study indicated a trivial change in the spreading width where the amplitude of U_z fluctuation was varied ±1%, ±3%, and ±5% about the mean. Table 3 outlines the results of the sensitivity study.

The velocity and pressure boundary conditions used for the CFD simulation cases are elucidated in Table 4.

Table 5 outlines the operational details of the CFD simulations performed in this study.

Open-source message passing interface (Open-MPI) was used for interprocessor communications on a server with 96 cores (four connected, 24-core Intel® Xeon® Processor nodes).

Results

A two-dimensional precursor test was undertaken to provide an estimate for the necessary mesh resolution to be used in the refinement zones for the final three-dimensional study. Although turbulence is essentially a three-dimensional phenomenon and LES is not strictly applicable to a two-dimensional approach [13], such an approach helps to provide an approximate starting point for the three-dimensional test case mesh generation. The precursor test was run for the maximum Reynolds number case from configuration A (corresponding to 5 bar). Three sequentially refined uniform mesh resolutions (0.5 mm, 0.4 mm, and 0.3 mm cell edge-length) were used for the precursor test to identify the optimal level of mesh refinement, based on the following criteria:

(1) The LES quality metric (γ) must be greater than 80% at the selected probe locations in the flow field [2,8]. An ideal indicator of the quality of the LES results would be a comparison with direct numerical simulation (DNS)—in the absence of which the LES quality metric serves as an estimate of the simulation quality. The LES quality metric is defined as

$$\gamma = \frac{\text{TKE}_{\text{resolved}}}{\text{TKE}_{\text{resolved}} + K_{\text{sgs}}} = \frac{0.5\langle u_i'' u_i'' \rangle}{0.5\langle u_i'' u_i'' \rangle + K_{\text{sgs}}} \tag{20}$$

$$u_i'' = U_i - \langle U_i \rangle$$

(2) The oil jet spreading width at TDC should conform within tolerance (±10%) to the experimental measurements.

Two probe locations were selected for the evaluation of the LES quality metric for the two-dimensional precursor test. The entry

Table 6 Two-dimensional precursor test results

Case	Cell edge-length (mm)	CFD spreading width (mm)	Actual spreading width (mm)	LES quality metric (γ)	
				Probe location (1)	Probe location (2)
5 bar	0.50	28	32	84.09%	96.47%
5 bar	0.40	30		92.44%	96.98%
5 bar	0.30	33		96.39%	98.18%

point of the oil into the cylindrical plenum (same as the exit point of the oil from the PCN) is defined as the reference point and is located at ($X = 0$, $Y = 0$) in the mesh geometry. Probe location 1 is situated 90 mm downstream of the reference point and approximates the end of the initial development region for the oil jet (25 d–30 d [2]). For the present study, this point is also perceived as the approximate initiation of the turbulent breakup regime for the oil jet. Probe location 2 is situated 283 mm downstream of the reference point and represents the TDC position of the piston. The spreading width of the oil jet is compared to that of the experiment at the TDC location. Averaging for the LES quality metric calculation is started after 60 ms of simulation time (approximately five flow-throughs for the 5 bar case) and is performed for another 60 ms. Precursor test results are documented in Table 6.

Although the LES quality metric values in Table 6 meet the Pope criterion [2,8], it is deemed only as a necessary but not sufficient condition since a two-dimensional approach cannot approximate the essentially three-dimensional turbulence physics. The precursor test therefore serves the sole purpose of providing a starting point for the three-dimensional test case mesh generation. From the precursor test results, a mesh resolution of 0.3 mm was observed to satisfy the LES quality metric criterion at both the probe locations and also predict the oil jet spreading width in closest approximation to the experimental data. The integral length-scale (l_0—assumed to be equal to d) is therefore resolved by 12 cells in the mesh, conforming to the guideline for optimum LES mesh resolution to resolve the integral length scale with 10–12 cells [14–17]. It is assumed that a mesh capable of resolving a majority of the TKE for the maximum Reynolds number case in configuration A will also satisfy the same requirement for all the other cases corresponding to lower Reynolds numbers. This allows for the use of the same mesh for all the three-dimensional test cases in configuration A.

The optimum mesh resolution identified from the precursor test is only applied in the refinement zones of the three-dimensional mesh as outlined in Fig. 3. In contrast to the precursor test, the three-dimensional test case therefore has nonuniform mesh spacing. While the outer unrefined zones are assumed to contribute trivially to the oil jet breakup phenomenon, their presence is essential to seclude any numerical effects of the domain boundaries on the free shear surface under study.

For the three-dimensional test cases, a base mesh of 1.2 mm cell edge-length is used and a level 2 zonal refinement (dividing each cell edge in 2^2) is performed on the base mesh. The oil jet spreading width results of the three-dimensional simulation test cases are documented in Table 7.

Figures 4–6 showcase the comparison between the CFD simulation and experimental test results for the oil jet spreading width.

Table 7 Three-dimensional CFD test case results

Case	Cell edge-length (mm)	CFD spreading width (mm)	Actual spreading width (mm)
1 bar	0.30	18	20
3 bar	0.30	25	26
5 bar	0.30	30	32

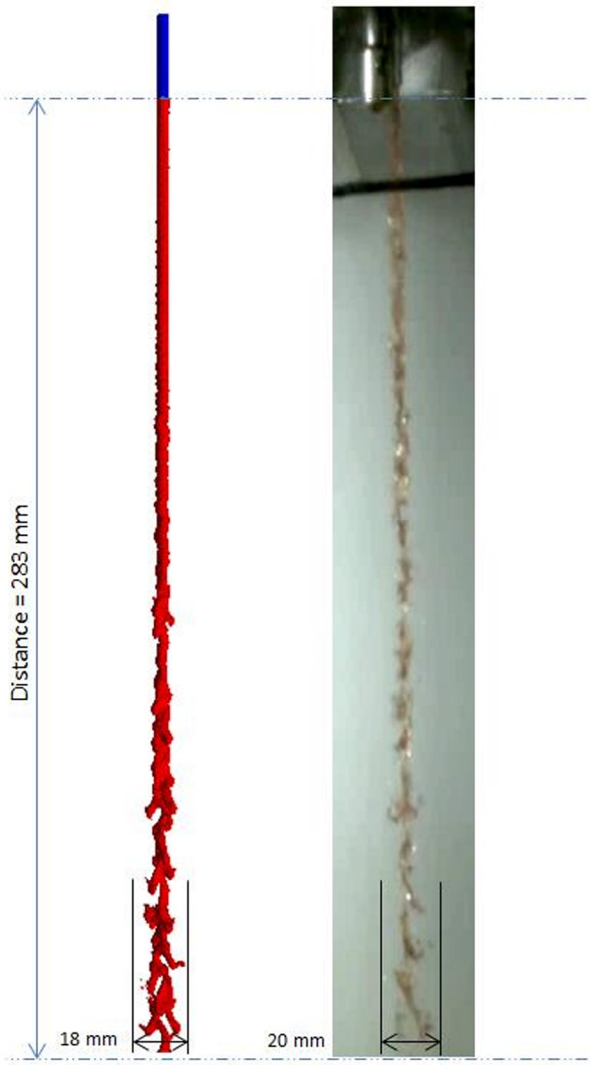

Fig. 4 One bar CFD and experimental oil jet spreading

The oil phase in the simulation results is represented using a phase-fraction filter of 0.1–1.

For the three-dimensional test cases, a series of probe locations were used to measure the LES quality metric defined in Eq. (20). In addition to the reference point ($X = 0$, $Y = 0$, $Z = 0$), other probe locations were selected 30 mm, 90 mm (~25 d), 130 mm, 180 mm, 230 mm, and 283 mm (TDC) downstream along the axis of the oil jet (Z-axis). Table 8 documents the LES quality metric measurements at the various probe locations.

For all the three test cases (with the exception of the 1 bar test case at the 90 mm probe location), the LES quality metric exceeds 80% downstream of the approximate breakup initiation point—signifying sufficient mesh resolution. It must however be noted that these values are arrived at after averaging velocity variables for all the three test cases for the same duration (60 ms) of

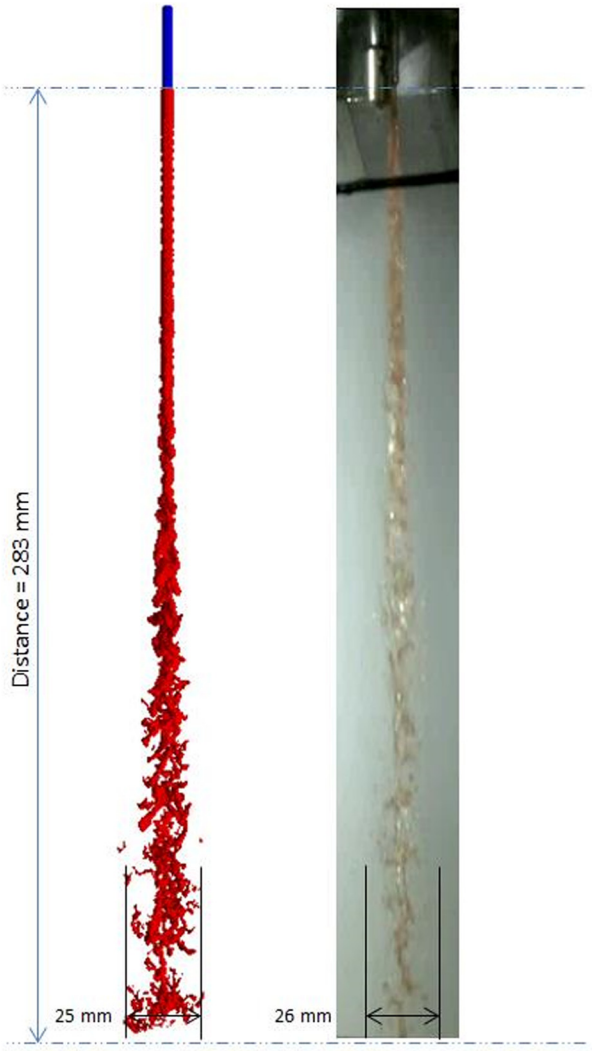

Fig. 5 Three bar CFD and experimental oil jet spreading

Fig. 6 Five bar CFD and experimental oil jet spreading

simulation time. For the 5 bar test case, this duration corresponds to approximately five flow-throughs, while for the 3 bar and 1 bar test cases it corresponds to approximately four and two flow-throughs, respectively. To get a more accurate average for the lower Reynolds number test cases, larger sample sets (corresponding to longer sampling durations) are required. A better comparison would average for an equal number of multiple flow-throughs for all the three test cases—in the absence of resources such an exercise was not undertaken for the present study.

Upstream of the approximate breakup initiation point, the LES quality metric is observed to be less than 80% in all the cases—indicating insufficiency of the mesh resolution in this region to resolve the largest energy producing scales of turbulence. The turbulence in the oil jet bulk is assumed to be dominated by small spatial scales in this region of the flow field—an effect that may be attributed to the initial wall-bounded flow regime inside the PCN. As per the KH theory, instabilities in the oil jet and their interaction with the surrounding air enlarge the length scales of turbulence in the flow field. This effect can be observed downstream of the breakup initiation point—as the mesh provides sufficient refinement to resolve a majority of the TKE (LES quality metric greater than 80%) at all the probe locations. In the scope of this study, we are interested in studying the effects of turbulence induced due to the interaction of oil and air that lead to the breakup of the oil jet. It therefore serves the purpose of this study to only have sufficient mesh resolution downstream of the breakup initiation point.

Table 8 LES quality metric (γ) measurements at probe locations for three-dimensional CFD test cases

Downstream probe location	1 bar	3 bar	5 bar
0 mm (PCN exit)	3.85%	5.65%	6.65%
30 mm	3.37%	8.87%	12.38%
90 mm	73.50%	84.82%	86.03%
130 mm	82.86%	84.69%	88.18%
180 mm	83.66%	87.96%	88.11%
230 mm	83.79%	88.53%	90.46%
283 mm (TDC)	91.52%	88.33%	89.95%

Figure 7 represents the LES quality metric for all the three-dimensional test cases at probe locations downstream of the approximate oil jet breakup initiation point.

The TKE spectrum is plotted in the wavenumber domain for the streamwise component of velocity (U_z) along the centerline of the oil jet flow field ($X = 0$, $Y = 0$). The sampling points are located 0.3 mm apart at each cell center between $Z = 0$ (PCN exit) and $Z = 300$ mm (end of computational domain). The averaged TKE (E) spectrum is plotted against the wavenumber (k) vector with the sample sets used for averaging spaced 5 ms apart between 65 ms and 120 ms of simulation time. The velocity vector used for

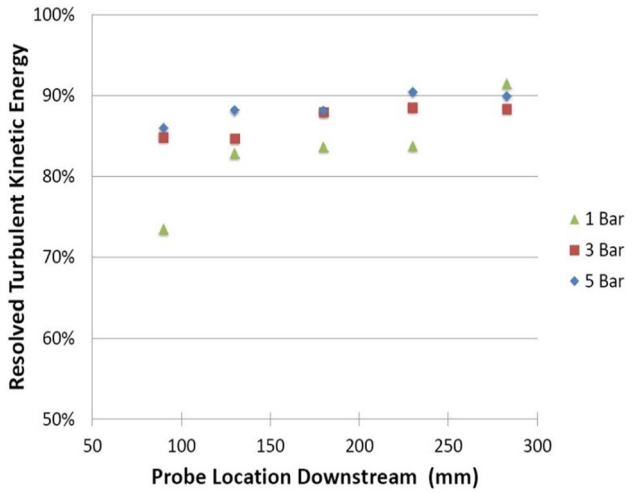

Fig. 7 LES quality metric (γ) at probe locations downstream of the oil jet breakup initiation point

calculating the TKE spectrum is made nondimensional by the inlet velocity for the corresponding test case. Figures 8–10 represent the averaged TKE spectra for the three-dimensional test cases in configuration A.

For each of the three-dimensional test cases, the TKE spectrum exhibits an approximately $(-5/3)$ slope in the wavenumber space corresponding to the inertial subrange length scales ($l_{DI} < l < l_{EI}$) in the turbulence energy cascade. The TKE spectrum thus validates the adequacy of the mesh resolution by conforming to the rate of energy transfer (proportional to $k^{-5/3}$) from the energy producing larger eddies to the dissipative smaller eddies, as described by the Kolmogorov theory [18].

Future Work

The simulation of oil jet spreading accounts for the primary step in the determination of the filling ratio of the piston cooling gallery. In engine operating conditions, the piston cooling gallery is in relative motion to the stationary PCN. Making the dynamic (moving) piston cooling gallery a part of the oil jet simulation increases the complexity owing to the mesh deformation (therefore simulation quality) considerations. A novel method to decouple the oil jet and piston cooling gallery dynamic motion simulation is therefore adopted.

In the first stage of this methodology, the oil jet spreading width is determined at various heights between bottom dead center (BDC) and TDC using the CFD simulation framework developed

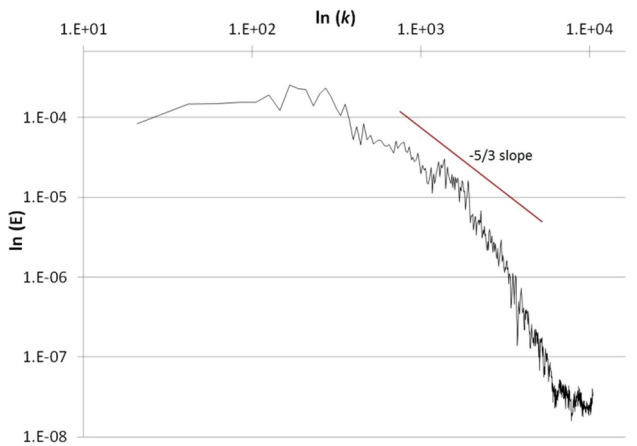

Fig. 8 TKE spectrum for the 1 bar case

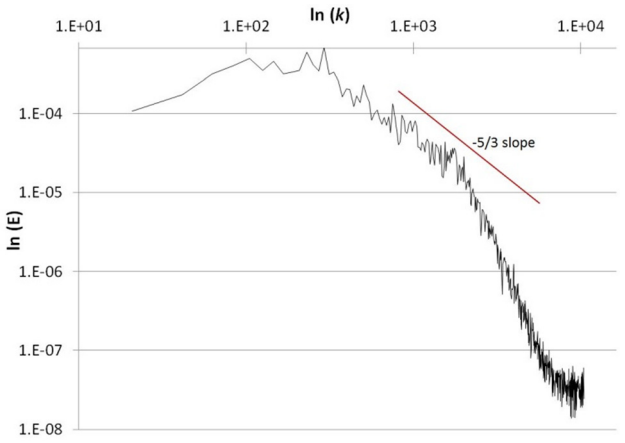

Fig. 9 TKE spectrum for the 3 bar case

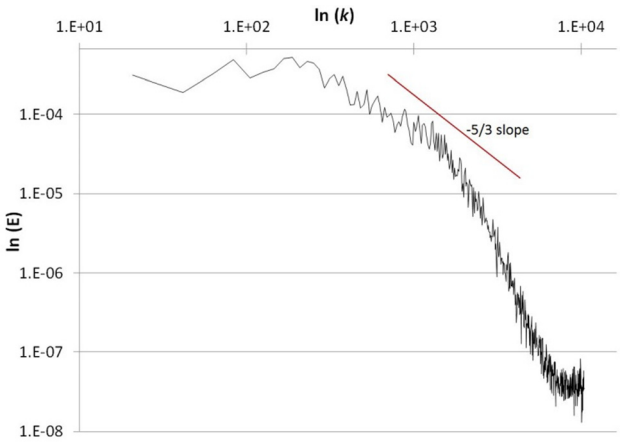

Fig. 10 TKE spectrum for the 5 bar case

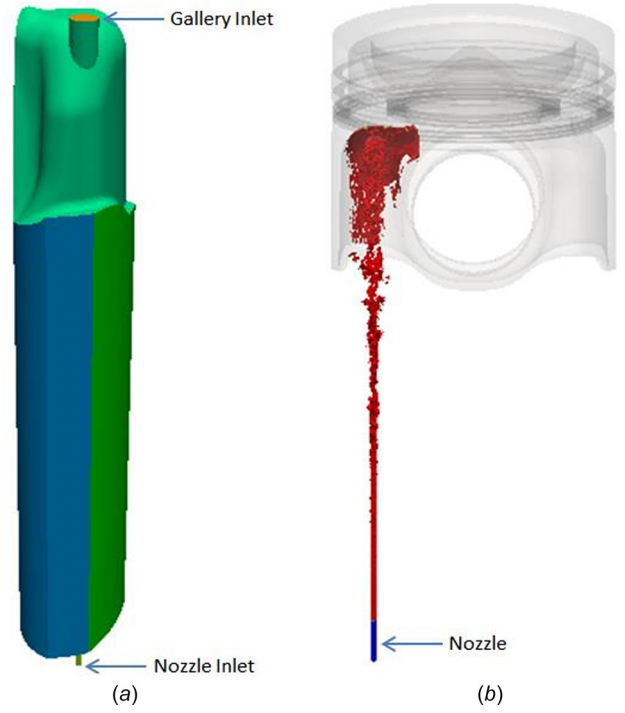

Fig. 11 (*a*) STL file representing the case geometry with piston cooling gallery inlet at TDC and (*b*) oil jet with piston cooling gallery inlet at TDC (piston shown only for representation)

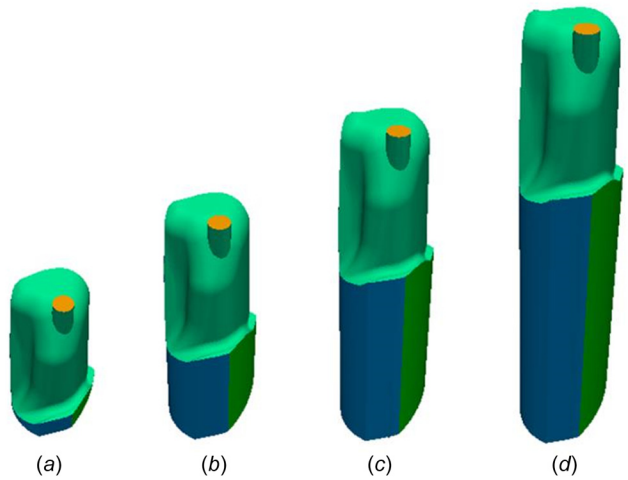

Fig. 12 STL geometry with piston cooling gallery at (*a*) BDC, (*b*) 25% of the stroke, (*c*) 50% of the stroke, and (*d*) 75% of the stroke

and validated in the Simulation Case Setup and Results sections. The computational domain is partly modeled as the undercrown of the piston. The inlet to the piston cooling gallery forms one of the boundary patches of the computational domain. The mass flow rate through this boundary patch is monitored to calculate the catching efficiency at these different heights. Figure 11 illustrates a sample case with the piston cooling gallery inlet at TDC.

Based on the catching efficiency calculations in the first stage, a boundary condition is formulated that varies the oil mass flow-rate at the piston cooling gallery inlet with the instantaneous stroke fraction of the piston. In addition to the geometry illustrated in Fig. 11(*a*), Fig. 12 illustrates other sample cases (at different stroke fractions) that can be used for the formulation of the aforementioned inlet boundary condition.

In the second stage of this methodology, dynamic mesh motion is applied to the piston cooling gallery case and the simulation is run until the filling ratio attains a pseudo steady-state value (the filling ratio oscillates in a narrow band since the piston is in continuous oscillatory motion). The determination of the filling ratio using this two-stage approach and subsequent validation of the simulation results with experimental data are the main objectives of the future CFD simulation work.

Conclusions

The oil jet spreading phenomenon has been studied for three test cases using the open-source CFD code OpenFoam®. The oil jet spreading width results predicted by the simulations agree with those obtained from the in-house experiments within a tolerance of ±10% deemed satisfactory for this study.

The adequacy of the mesh resolution for LES has been validated using the LES quality metric, which is a measure of the fraction of the TKE resolved by the simulation [8]. Probe locations downstream of the breakup initiation point along the flow axis indicate more than 80% resolution of the TKE, signifying sufficient mesh resolution to capture a majority of the energy producing length scales of turbulence in accordance with the guideline for a well-resolved LES [2]. The LES quality metric results indicate that the wall-bounded (inside the PCN) and the near PCN-exit regions of the mesh are incapable of resolving these length scales in sufficient detail. Due to the lack of majority TKE resolution throughout the flow field, this simulation study can therefore be classified as a very large eddy simulation (VLES) [2].

The TKE spectral analysis for the streamwise velocity component (U_z) reveals an approximately (−5/3) slope in the wavenumber space corresponding to the inertial length scales of turbulence, thus indicating a transfer of energy from the larger energy producing scales to the smaller dissipative scales at a rate conforming to that dictated by the Kolmogorov theory [18].

The numerical setup developed for the present CFD simulation study is capable of providing physically accurate predictions for the oil jet spreading width. The setup can be used to formulate the inlet boundary condition for the dynamic mesh piston cooling gallery CFD simulation, yielding the filling ratio. Knowledge of the filling ratio can help the empirical deduction of the piston cooling gallery HTCs. The numerical setup for predicting the oil jet spreading serves as the primary stage in the envisioned development of a multistage in-house CFD simulation tool for piston cooling gallery design.

Acknowledgment

The authors would like to acknowledge the support extended by Mr. Jindrich Hofirek, Research Europe—Laboratories, MAHLE International GmbH (Stuttgart) and Dr. Kyle Mooney, ICON Technology & Process Consulting.

Nomenclature

BDC = bottom dead center
CE = catching efficiency
CFD = computational fluid dynamics
d = PCN diameter (m)
DNS = direct numerical simulation
$E(k)$ = dimensionless turbulent kinetic energy
FR = filling ratio
FV = finite volume
HTC = heat transfer coefficient
k = wavenumber (m^{-1})
k_{sgs} = SGS turbulent kinetic energy ($m^2\ s^{-2}$)
l_{DI} = inertial to energy dissipation scale transition length (m)
l_{EI} = energy producing to inertial scale transition length (m)
l_0 = integral length scale (m)
LES = large eddy simulation
LPM = liters per minute
PCN = piston cooling nozzle
PCU = power cell unit
PISO = pressure implicit with splitting of operators
RANS = Reynolds-averaged Navier–Stokes
$\overline{\mathcal{S}}$ = filtered strain-rate invariant (s^{-1})
$\overline{S_{ij}}$ = filtered strain-rate tensor (s^{-1})
SGS = subgrid scale
SIMPLE = semi-implicit method for pressure-linked equations
STL = stereolithography
TDC = top dead center
TKE = turbulent kinetic energy
VLES = very large eddy simulation
γ = LES quality metric
Δ = LES spatial filter cutoff width (m)
δ_{ij} = Kronecker delta
ν = kinematic viscosity ($m^2\ s^{-1}$)
ν_{sgs} = SGS turbulent viscosity ($m^2\ s^{-1}$)
ρ = density ($kg\ m^{-3}$)
τ_{ij} = SGS stress tensor ($m^2\ s^{-2}$)
τ_0 = integral time-scale (s)
φ = scalar function

References

[1] Sroka, Z. J., 2012, "Some Aspects of Thermal Load and Operating Indexes After Downsizing for Internal Combustion Engine," J. Therm. Anal. Calorim., **110**(1), pp. 51–58.
[2] Pope, S. B., 2000, *Turbulent Flows*, 1st ed., Cambridge University Press, Cambridge, UK.
[3] Gohil, T. B., Saha, A. K., and Muralidhar, K., 2012, "Numerical Study of Instability Mechanisms in a Circular Jet at Low Reynolds Numbers," Comput. Fluids, **64**, pp. 1–18.

[4] Liepmann, D., and Gharib, M., 1992, "The Role of Streamwise Vorticity in the Near-Field Entrainment of Round Jets," J. Fluid Mech., **245**, pp. 643–668.
[5] Yule, A. J., 1978, "Large-Scale Structure in the Mixing Layer of a Round Jet," J. Fluid Mech., **89**(3), pp. 413–432.
[6] Brown, G. L., and Roshko, A., 1974, "On Density Effects and Large Structure in Turbulent Mixing Layers," J. Fluid Mech., **64**(4), pp. 775–816.
[7] Winant, C. D., and Browand, F. K., 1974, "Vortex Pairing: The Mechanism of Turbulent Mixing-Layer Growth at Moderate Reynolds Number," J. Fluid Mech., **63**(2), pp. 237–255.
[8] Pope, S. B., 2004, "Ten Questions Concerning the Large-Eddy Simulation of Turbulent Flows," New J. Phys., **6**(1), p. 35.
[9] Smagorinsky, J., 1963, "General Circulation Experiments With the Primitive Equations—I: The Basic Experiment," Mon. Weather Rev., **91**(3), pp. 99–164.
[10] De Villiers, E., 2007, "The Potential of Large Eddy Simulation for the Modelling of Wall Bounded Flows," Ph.D. dissertation, University of London, London, UK, pp. 65–66.
[11] Issa, R. I., 1986, "Solution of the Implicitly Discretised Fluid Flow Equations by Operator-Splitting," J. Comput. Phys., **62**(1), pp. 40–65.
[12] Patankar, S. V., and Brian Spalding, D., 1972, "A Calculation Procedure for Heat, Mass and Momentum Transfer in Three-Dimensional Parabolic Flows," Int. J. Heat Mass Transfer, **15**(10), pp. 1787–1806.
[13] Murakami, S., and Mochida, A., 1995, "On Turbulent Vortex Shedding Flow Past 2D Square Cylinder Predicted by CFD," J. Wind Eng. Ind. Aerodyn., **54–55**, pp. 191–211.
[14] Graham, P., 2014, "Experimental and Numerical Study of Multi-Phase Flow in a Coaxial Air Jet," Ph.D. dissertation, Queen's University, Kingston, ON, Canada, p. 105.
[15] Addad, Y., Benhamadouche, S., and Laurence, D., 2004, "The Negatively Buoyant Wall-Jet: LES Results," Int. J. Heat Fluid Flow, **25**(5), pp. 795–808.
[16] Baggett, J. S., Jiménez, J., and Kravchenko, A. G., 1997, "Resolution Requirements in Large-Eddy Simulations of Shear Flows," *Annual Research Briefs*, Center for Turbulence Research, Stanford, CA, pp. 51–66.
[17] Gant, S. E., 2010, "Reliability Issues of LES-Related Approaches in an Industrial Context," Flow Turbul. Combust., **84**(2), p. 325.
[18] Kolmogorov, A. N., 1991, "The Local Structure of Turbulence in Incompressible Viscous Fluid for Very Large Reynolds Numbers," Proc. Math. Phys. Sci., **434**(1890), pp. 9–13.